The Astrophysical Journal, 670:313–331, 2007 November 20

THE KINEMATICS OF THE ULTRA-FAINT MILKY WAY SATELLITES: SOLVING THE MISSING SATELLITE PROBLEM

Joshua D. Simon
Department of Astronomy, California Institute of Technology, 1200 East California Boulevard, MS 105-24, Pasadena, CA 91125; jsimon@astro.caltech.edu

and

Marla Geha[1]
National Research Council of Canada, Herzberg Institute of Astrophysics, 5071 West Saanich Road, Victoria, BC V9E 2E7, Canada; marla.geha@nrc-cnrc.gc.ca
Received 2007 May 18; accepted 2007 July 21

ABSTRACT

We present Keck DEIMOS spectroscopy of stars in eight of the newly discovered ultra-faint dwarf galaxies around the Milky Way. We measure the velocity dispersions of Canes Venatici I, Canes Venatici II, Coma Berenices, Hercules, Leo IV, Leo T, Ursa Major I, and Ursa Major II from the velocities of 18–214 stars in each galaxy and find dispersions ranging from 3.3 to 7.6 km s^{-1}. The six galaxies with absolute magnitudes $M_V < -4$ are highly dark matter dominated, with mass-to-light ratios approaching 1000 $M_\odot/L_{\odot,V}$. For the fainter galaxies we find tentative evidence for tidal disruption. The measured velocity dispersions of the ultra-faint dwarfs are correlated with their luminosities, indicating that a minimum mass for luminous galactic systems may not yet have been reached. We also measure the metallicities of the observed stars and find that the new dwarfs have mean metallicities of $[\mathrm{Fe/H}] = -2.0$ to -2.3; these galaxies represent some of the most metal-poor stellar systems known. The six brightest of the ultra-faint dwarfs extend the luminosity-metallicity relationship followed by more luminous dwarfs by a factor of $\sim$30 in luminosity. We detect metallicity spreads of up to 0.5 dex in several objects, suggesting multiple star formation epochs. UMa II and Com, despite their exceptionally low luminosities, have higher metallicities that suggest they may once have been much more massive. Having established the masses of the ultra-faint dwarfs, we re-examine the missing satellite problem. After correcting for the sky coverage of the Sloan Digital Sky Survey, we find that the ultra-faint dwarfs substantially alleviate the discrepancy between the predicted and observed numbers of satellites around the Milky Way, but there are still a factor of $\sim$4 too few dwarf galaxies over a significant range of masses. We show that if galaxy formation in low-mass dark matter halos is strongly suppressed after reionization, the simulated circular velocity function of CDM subhalos can be brought into approximate agreement with the observed circular velocity function of Milky Way satellite galaxies.

Subject headings: dark matter — galaxies: dwarf — galaxies: kinematics and dynamics — Local Group — techniques: radial velocities

Online material: color figure

1. INTRODUCTION

The cold dark matter (CDM) cosmological model predicts that massive galaxies such as the Milky Way should be surrounded by large numbers of dark matter dominated satellite halos. The relatively modest populations of observed dwarf galaxies orbiting the Milky Way and Andromeda, however, seem to conflict with this prediction (Kauffman et al. 1993; Klypin et al. 1999; Moore et al. 1999). This apparent disagreement between the expected and observed numbers of dwarf galaxies has become widely known as the "substructure" or "missing dwarf" problem.

Proposed solutions to the substructure problem can be broadly divided into two categories: cosmological and astrophysical. Cosmological solutions include modifying the power spectrum at small scales (Kamionkowski & Liddle 2000; Zentner & Bullock 2003) and changing the properties of the dark matter particles, such as by making them warm (Colín et al. 2000; Bode et al. 2001) or invoking a late decay from a nonrelativistic particle (Strigari et al. 2007b). Astrophysical solutions are more prosaic, but perhaps easier to constrain observationally. Some of the most popular astrophysical solutions include the hypothesis that reionization could suppress the formation of dwarf galaxies by preventing low-mass dark matter halos from acquiring enough gas to form stars after $z \sim 10$ (e.g., Bullock et al. 2000; Somerville 2002; Benson et al. 2002; Ricotti & Gnedin 2005; Moore et al. 2006) and the possibility that the dwarf galaxies we observe today were once much more massive objects that have been reduced to their present appearance by dramatic tidal stripping (Mayer et al. 2001a, 2001b; Kravtsov et al. 2004). Despite a wealth of ideas about how to solve the missing dwarf problem, distinguishing between the various proposals has proved to be difficult, and making sense of the tremendous variety of masses, luminosities, mass-to-light ratios, gas fractions, and star formation histories among observed dwarf galaxies remains a challenge.

Our understanding of the missing satellite problem and the evolution of dwarf galaxies is being rapidly revised by the discovery of a large population of new, very faint Local Group dwarfs in the Sloan Digital Sky Survey (SDSS; York et al. 2000) and other wide-field imaging surveys. In the past three years, at least 20 of these galaxies have been identified, nearly doubling the previously known population. The new dwarfs include eight additional Milky Way dwarf spheroidals (Willman et al. 2005a; Zucker et al. 2006a, 2006b; Belokurov et al. 2006, 2007b; Grillmair 2006;

[1] Current address: Astronomy Department, Yale University, New Haven, CT 06520; marla.geha@yale.edu.

TABLE 1
Observing Targets

Galaxy	α (J2000.0)	δ (J2000.0)	M_V	μ_V[a] (mag arcsec^{-2})	Distance[b] (kpc)	References
Ursa Major II	08 51 30.00	63 07 48.0	−3.8	28.8	32	1, 2
Leo T	09 34 53.40	17 03 05.0	−7.1	26.9	417	3
Ursa Major I	10 34 52.80	51 55 12.0	−5.6	28.9	106	4, 5, 6
Leo IV	11 32 57.00	−00 32 00.0	−5.1	28.3	158	2
Coma Berenices	12 26 59.00	23 54 15.0	−3.7	27.4	44	2
Canes Venatici II	12 57 10.00	34 19 15.0	−4.8	27.2	151	2
Canes Venatici I	13 28 03.50	33 33 21.0	−7.9	28.2	224	7
Hercules	16 31 02.00	12 47 30.0	−6.0	28.6	138	2

Note.—Units of right ascension are hours, minutes, and seconds, and units of declination are degrees, arcminutes, and arcseconds.
[a] Central surface brightnesses, calculated from the Plummer profile fit parameters given in the cited discovery papers.
[b] The distances reported in the literature for these galaxies have generally been rounded off to the nearest multiple of 10 kpc after converting from the distance modulus, which is the quantity directly constrained by the data. The distances listed here have been calculated from the published distance moduli and rounded to the nearest kpc.
References.—(1) Zucker et al. 2006b; (2) Belokurov et al. 2007b; (3) Irwin et al. 2007; (4) Willman et al. 2005a; (5) Belokurov et al. 2006; (6) this work; (7) Zucker et al. 2006a.

Sakamoto & Hasegawa 2006) and one dwarf irregular (Irwin et al. 2007), eight new dwarf spheroidals around Andromeda (Zucker et al. 2004, 2007; Martin et al. 2006; Majewski et al. 2007; Ibata et al. 2007), and three further new Milky Way satellites that lie in the uncertain parameter space between dwarf galaxies and globular clusters (Willman et al. 2005b; Belokurov et al. 2007b; Walsh et al. 2007). Nearly all of these objects have both surface brightnesses and luminosities that are significantly lower than those of any previously known galaxies.

Properly placing these new discoveries within the framework of CDM and the missing satellite problem requires measurements of their internal kinematics, in order to determine whether the ultra-faint dwarfs are gravitationally bound, dark matter dominated galaxies, or tidally disrupted systems. Only five of these objects (Ursa Major I, Andromeda IX, Boötes, Canes Venatici I, and Andromeda XIV) have published stellar kinematics measurements, and for two of the three ultra-faint Milky Way dwarfs that have been studied already only a handful of stars were observed (Kleyna et al. 2005; Chapman et al. 2005; Muñoz et al. 2006a; Ibata et al. 2006; Majewski et al. 2007). In this paper, we present new stellar velocity measurements of larger samples of stars in eight of the 12 new Milky Way satellites (see Table 1). Including the other published studies and studies in preparation that we are aware of, the only known Milky Way satellites that remain unobserved are Segue 1 and Boötes II.

In § 2, we describe our observations, target selection, and data reduction, focusing in particular on our techniques for obtaining very high precision velocity measurements with the Deep Imaging Multi-Object Spectrograph (DEIMOS). We present the main results of this study, including measured velocity dispersions, masses, mass-to-light ratios, and metallicities in § 3. In § 4, we discuss the implications of our results for the CDM model and the missing satellite problem. We summarize our results and conclusions in § 5.

2. OBSERVATIONS AND DATA REDUCTION

2.1. *Observations*

We obtained spectra of individual stars in eight dwarf galaxies with the DEIMOS spectrograph (Faber et al. 2003) on the Keck II telescope on 2007 February 12–14. During the observations, the weather was clear, with seeing that varied between 0.5″ and 0.9″ (with a very brief excursion to 1.4″). The spectrograph was configured to cover the wavelength range 6500–9000 Å with the 1200 line mm^{-1} grating, and the OG550 filter was used to block shorter wavelength light. The spectral dispersion of this setup is 0.33 Å pixel^{-1}, and the resulting spectral resolution, taking into account our slit width of 0.7″ and the anamorphic distortion factor of 0.7, is 1.37 Å FWHM (corresponding to 12 km s^{-1} pixel^{-1} and 47 km s^{-1} FWHM at the Ca II triplet). Exposures of Kr, Ar, Ne, and Xe arc lamps provided the wavelength calibration, and an internal quartz lamp was used for flat-fielding.

We observed 18 DEIMOS slit masks, with total exposure times ranging between 20 minutes and 2.5 hr. One to four masks were placed on each galaxy. Each mask contained ∼50–100 stars, of which ∼30%–80% were expected to be actual members of the target galaxies from the SDSS photometry. The positions, exposure times, and number of slits on each mask are listed in Table 2. Typical target stars had magnitudes of $r \approx 20$–21. At $r = 20$, a 1 hr exposure in good seeing conditions yields a signal-to-noise ratio (S/N) of ∼15, and a 2.5 hr exposure gives a S/N of ∼22, where the S/N is calculated as the average S/N per pixel in the Ca II triplet region.

Target selection was carried out on star catalogs extracted from the NYU-VAGC analysis (Blanton et al. 2005) of the Sloan Digital Sky Survey Data Release 5 data set (Adelman-McCarthy et al. 2007).[2] We set the target priorities so as to preferentially observe stars with a high likelihood of being members of the various dwarfs based on their color, apparent magnitude, and position. We constructed r, $g - i$ color-magnitude diagrams (CMDs) for each dwarf and overlaid globular cluster isochrones from Clem (2005, hereafter C05), adjusted for the distance reported in the literature. We chose the best-fitting globular cluster red giant branch (RGB) of the three examples provided by C05. We also added a horizontal branch track derived from the M13 observations of C05 and asymptotic giant branch (AGB) isochrones (for an age of 11.2 Gyr and a metallicity of [Fe/H] = −1.3 or [Fe/H] = −1.7) from Girardi et al. (2004). The highest priority targets were those located within 0.1 mag (in the least-squares sense[3]) of the RGB or AGB tracks, or within 0.2 mag of the horizontal branch, with additional preference being given to brighter stars. Stars farther from any of the

[2] The position of Leo T, which was discovered during our observing preparations, had not yet been processed for the VAGC at that time, so to select targets for that galaxy we used the standard DR5 data.

[3] As in § 3.1, when we refer to the distance between a star and a fiducial track in a color-magnitude diagram, we mean the following: $d_{\rm CMD} = \{[(g-i)_* - (g-i)_{\rm fiducial}]^2 + (r_* - r_{\rm fiducial})^2\}^{1/2}$, where the appropriate reference point for each star along the fiducial track is chosen so as to minimize $d_{\rm CMD}$.

TABLE 2
KECK DEIMOS SLIT MASK OBSERVING PARAMETERS

Mask Name	α (J2000.0)	δ (J2000.0)	P.A. (deg)	t_{exp} (s)	Number of Slits	Percent Useful Spectra
UMaII-1	08 50 38.68	63 06 45.0	95.8	3600	81	48%
UMaII-2	08 49 42.19	63 11 05.6	180.0	3600	87	52%
UMaII-3	08 53 08.75	63 04 45.4	109.0	2400	76	62%
UMaI-1	10 34 50.57	51 54 47.7	65.0	5400	68	59%
UMaI-2	10 34 22.23	51 56 23.9	66.0	3600	62	65%
UMaI-3	10 35 35.62	51 56 06.4	23.3	5400	68	85%
LeoT-1	09 35 00.18	17 00 56.3	1.0	3600	87	75%
LeoIV-1	11 32 58.69	−00 31 41.1	9.8	3000	77	83%
ComBer-1	12 27 08.32	23 52 52.0	117.0	9000	78	62%
ComBer-2	12 26 44.48	23 57 58.7	140.0	9000	78	51%
ComBer-3	12 26 47.98	23 54 42.8	−20.0	9000	80	65%
CVnII-1	12 57 12.78	34 20 43.8	−20.0	9000	67	81%
CVnII-2	12 57 16.03	34 18 51.8	50.0	1200	66	30%
CVnI-1	13 27 59.38	33 34 26.8	73.0	4140	91	87%
CVnI-2	13 28 09.19	33 31 16.0	70.5	4140	94	83%
CVnI-3	13 28 14.34	33 33 23.3	−2.0	4860	90	83%
CVnI-4	13 28 02.17	33 33 36.7	−112.0	9000	115	79%
Herc-1	16 31 02.70	12 47 21.3	104.0	4500	106	83%

NOTES.—Mask name, right ascension, declination, position angle, and total exposure time for each Keck DEIMOS slit mask. Units of right ascension are hours, minutes, and seconds, and units of declination are degrees, arcminutes, and arcseconds. The final two columns refer to the total number of slitlets on each mask and the percentage of those slitlets for which a redshift was measured.

fiducial sequences were classified as lower priority targets. We then designed slit masks so as to maximize the number of high-priority targets while still obtaining good spatial coverage. Slit masks were created using the DEIMOS `dsimulator` slit-mask design software, which fills in the mask area to the extent possible with the highest priority input targets. This automatic selection was then adjusted by hand as appropriate. The remaining space on the slit masks was filled in with lower priority targets. The slit width for all masks was $0.7''$, and the minimum slit lengths were $\sim 5''$, depending slightly on the density of target stars.

In addition to the dwarf galaxy observations, we also obtained spectra of a radial velocity standard star, several telluric standards, and stars in the globular cluster NGC 1904 to serve as templates for cross-correlation with the dSph stars. More template observations (the globular cluster NGC 2419 and other radial velocity standards) were obtained during additional recent Keck DEIMOS observing runs, with identical observing setups (except for the slit width).

2.2. *Data Reduction*

The data were reduced using version 1.1.4 of the DEIMOS data reduction pipeline developed for the DEEP2 Galaxy Redshift Survey (M. C. Cooper 2007, private communication). Since this software was designed for faint, resolved galaxies, we modified the pipeline to optimize reductions for our relatively bright unresolved stellar targets. The main modifications were to change the cosmic-ray rejection algorithm and to allow alignment of individual two-dimensional exposures in the spatial direction before co-adding. In addition, we modified the long-slit pipeline to allow proper reduction of very bright standard stars.

2.3. *Measurement of Radial Velocities*

We measure radial velocities by cross-correlating the observed science spectra with a set of high-S/N stellar templates. The stellar templates were observed with Keck DEIMOS using the same setup described above. Because template mismatch can result in significant velocity errors, we include a wide variety of stellar types and metallicities in our template library: giants of spectral type F8 III through M8 III, subgiants, and dwarf stars. In order to cover the range of metallicity expected in our low-luminosity dwarf galaxies, we also include several RGB and horizontal branch (HB) stars taken from observations of Galactic globular clusters. The stellar templates cover the metallicity range $[\mathrm{Fe/H}] = -2.12$ to +0.11. All science and template spectra are rebinned onto a common wavelength array with logarithmic wavelength bins of size 15 km s^{-1} pixel^{-1}, which is chosen to match the lowest spectral resolution present in the observed data.

We calculate and apply a telluric correction to each velocity measurement to account for velocity errors that result from mis-centering an unresolved star within the slit. Following Sohn et al. (2007), we cross-correlate each science spectrum with a telluric template in the regions of the strong telluric absorption: 6860–6925, 7167–7320, 7593–7690, and 8110–8320 Å. The telluric template was created from the spectrum of a hot, rapidly rotating star (HR 1641, B3 V) that was allowed to drift perpendicularly across the slit (i.e., across the $0.7''$ dimension) during the exposure, simulating a source that uniformly fills the slit, and thus accurately reflects the mean integrated slit function. The mean telluric offset per mask ranged between −7 and +2 km s^{-1}, with a standard deviation within a mask of 3 km s^{-1}. This correction is the velocity error caused by the mis-centering of the science star within the slit from, e.g., astrometry errors, or small mask rotation. Repeat observations of a number of stars on multiple masks demonstrate that the telluric correction reduces the mean absolute deviation between independent pairs of measurements from 4.6 to 3.8 km s^{-1}, reduces the weighted standard deviation of the velocity differences between pairs of measurements from 5.6 to 4.2 km s^{-1}, and improves the weighted mean difference from −2.0 to −0.4 km s^{-1}, indicating that the telluric correction is removing both random and systematic errors from the data.

We first calculate the telluric offset (v_{tell}) and then determine radial velocities (v_{obs}) for each science spectrum. In both cases, the template and science spectra are continuum subtracted; the template is then shifted and scaled to find the best fit in reduced-χ^2

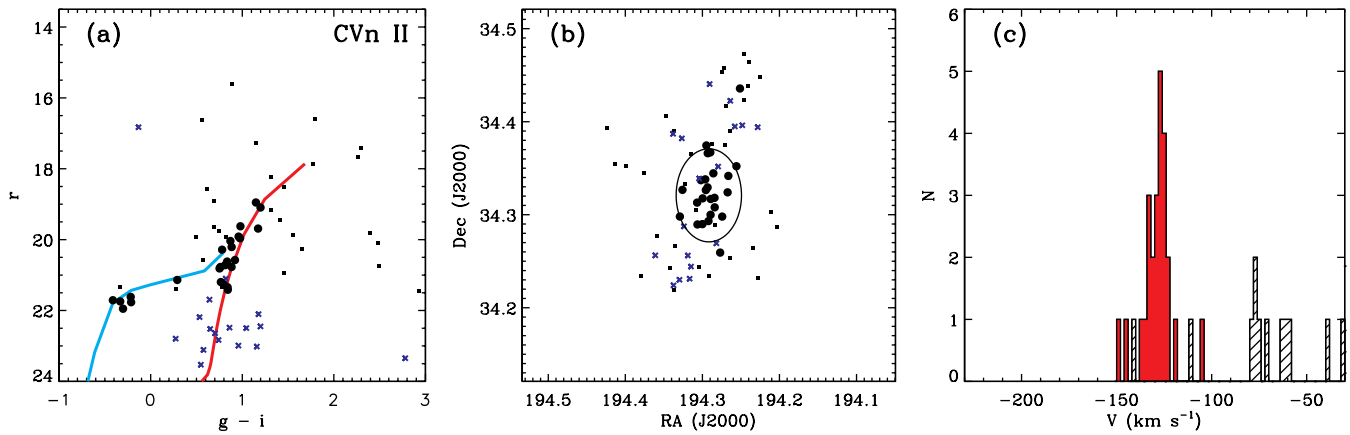

FIG. 7.—Same as Fig. 2, but for Canes Venatici II.

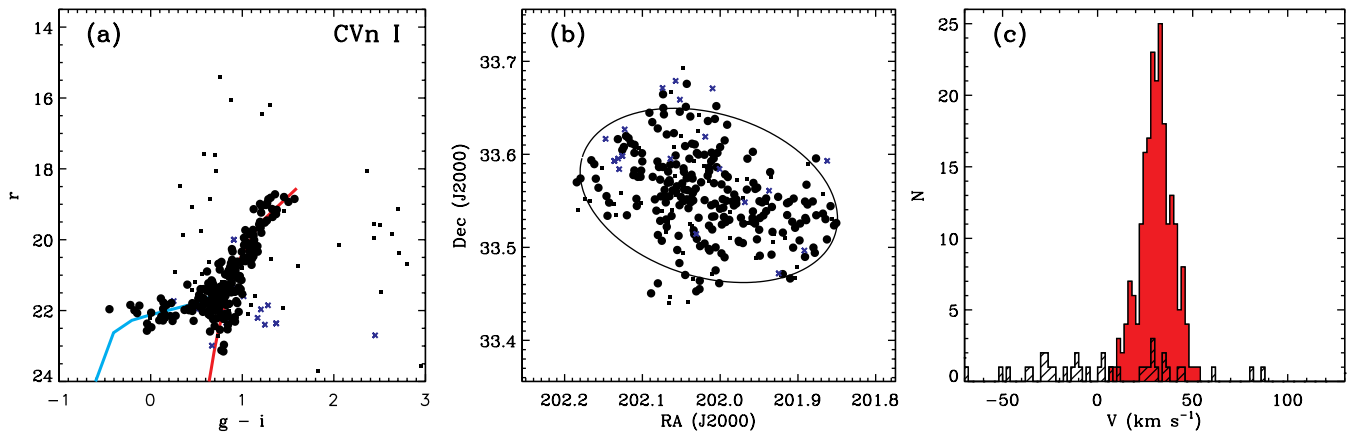

FIG. 8.—Same as Fig. 2, but for Canes Venatici I.

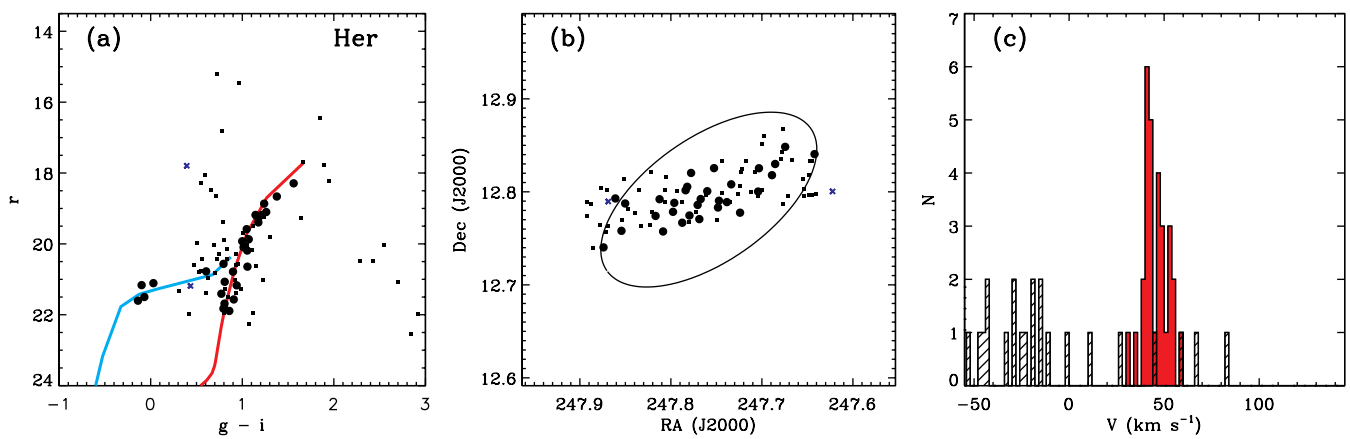

FIG. 9.—Same as Fig. 2, but for Hercules.

TABLE 3
RADIAL VELOCITIES AND VELOCITY DISPERSIONS

Galaxy	$\langle\hat{u}\rangle_{\rm hel}$ (km s^{-1})	$d\langle\hat{u}\rangle_{\rm hel}$ (km s^{-1})	$\langle\hat{u}\rangle_{\rm GSR}$ (km s^{-1})	σ (km s^{-1})	$d\sigma$ (km s^{-1})	Number of Stars
Ursa Major II	−116.5	1.9	−33.4	6.7	1.4	20
Leo T	38.1	2.0	−58.4	7.5	1.6	19
Ursa Major I	−55.3	1.4	−7.1	7.6	1.0	39
Leo IV	132.3	1.4	10.1	3.3	1.7	18
Coma Berenices	98.1	0.9	81.7	4.6	0.8	59
Canes Venatici II	−128.9	1.2	−95.5	4.6	1.0	25
Canes Venatici I	30.9	0.6	77.6	7.6	0.4	214
Hercules	45.0	1.1	144.6	5.1	0.9	30

between 0.2 and 0.3 for relevant binary periods), Olszewski et al. suggested that the velocity dispersion from binaries alone is on the order of 1.5 km s^{-1}. Since it is possible that the binary fractions may be different in the lower luminosity galaxies we observed, we use this estimate only as a guide. For the highest velocity dispersion systems listed in Table 3, the effect of binaries is negligible. This result is consistent with conclusions from previous groups for other Local Group dSphs (Kleyna et al. 1999; Walker et al. 2006a). For our lowest dispersion system, Leo IV, the Olszewski et al. binary correction would reduce the measured dispersion from 3.3 to 2.9 km s^{-1}. However, this difference is significantly smaller than our measurement uncertainty of 1.7 km s^{-1}, so we do not correct our measured dispersions for the presence of binaries. Unless the binary star fraction in these ultra-low luminosity dwarfs is significantly larger than that of other dwarf galaxies, binaries do not significantly inflate the measured dispersions and inferred masses of even the lowest dispersion dwarf galaxies in our sample.

3.3. *Total Masses*

The process of determining the total mass of a dwarf spheroidal galaxy from the velocities of a relatively modest sample of stars that are probably located well inside the virial radius of the galaxy's dark matter halo is fraught with difficulty. The standard technique in the literature is to assume that (1) the galaxy is spherical; (2) the galaxy is in dynamical equilibrium; (3) the galaxy has an isotropic velocity dispersion; and (4) the light distribution of the galaxy traces its mass distribution. All four of these assumptions may be false in reality, especially for the ultra-faint dwarfs that are the subject of this paper. SDSS photometry and follow-up imaging reveal that most of the dwarfs are elongated, demonstrating that they are not spherically symmetric systems and probably do not have isotropic velocity dispersion tensors. Several of the dwarfs also appear irregular, opening up the possibility that their structure has been significantly affected by the tidal field of the Milky Way. However, these apparently irregular isodensity contours could also be the result of the extremely low surface densities of the galaxies, which make their stellar distributions difficult to determine accurately. Finally, the nearly flat velocity dispersion profiles observed in all of the dSphs where spatially resolved kinematics are available indicate that light does not trace mass (Walker et al. 2006a; Wu 2007). Despite these objections, the samples of stars in the ultra-faint dwarfs that are spectroscopically accessible with current instruments are so small that more sophisticated analyses are not possible (with the exception of CVn I, which will be discussed in more detail in a future paper). We therefore use the method of Illingworth (1976) to estimate total masses for the observed galaxies:

$$M_{\rm tot} = 167\beta r_c \sigma^2, \tag{3}$$

where β is a parameter that depends on the concentration of the system and is generally assumed to be 8 for dSphs (Mateo 1998), r_c is the King (1962) profile core radius, and σ is the observed central velocity dispersion. For most of the new dwarfs, only Plummer

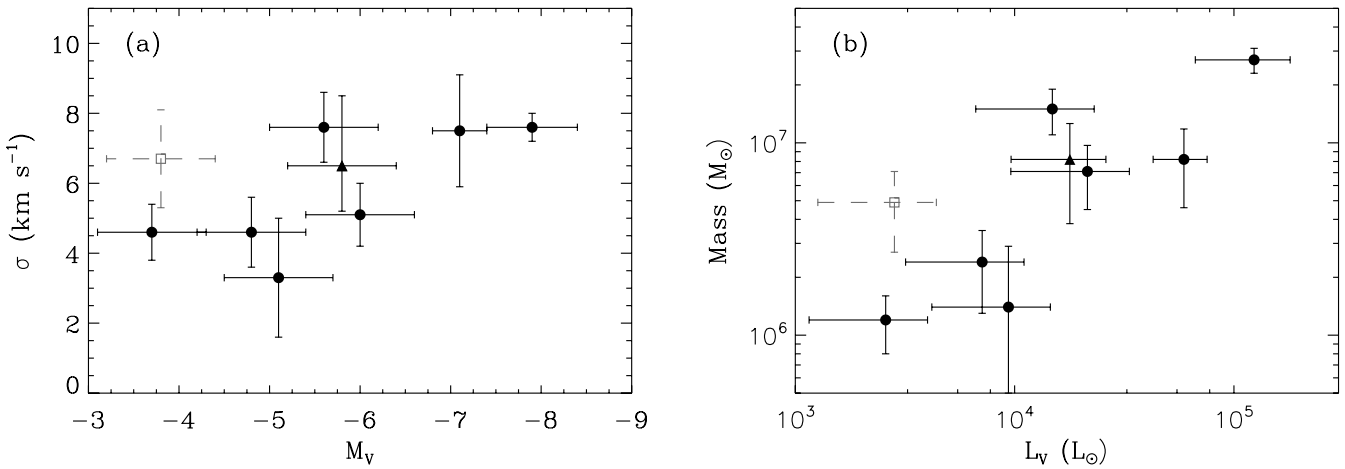

FIG. 10.—(*a*) Velocity dispersion as a function of absolute magnitude for the ultra-faint dwarfs. The filled black symbols represent the gravitationally bound dwarfs and the open gray symbol represents UMa II, which is thought to be tidally disrupted (see § 3.6). Circles are ultra-faint dwarfs in this sample and the triangle is the Boötes dSph (Martin et al. 2007). (*b*) Dynamical mass as a function of total *V*-band luminosity. Symbols are the same as in (*a*). The ultra-faint dwarf galaxies clearly display a trend in which the more luminous galaxies have larger velocity dispersions and correspondingly larger masses. Perhaps surprisingly, there appears to be a simple power-law relationship between mass and luminosity.

TABLE 4
Masses, Mass-to-Light Ratios, and Metallicities

Galaxy	Mass ($M_\odot$)	M/L_V ($M_\odot/L_\odot$)	[Fe/H]	$\sigma_{[Fe/H]}$
Ursa Major II[a]	$(4.9 \pm 2.2) \times 10^6$	1722 ± 1226	-1.97 ± 0.15	0.28
Leo T	$(8.2 \pm 3.6) \times 10^6$	138 ± 71	-2.29 ± 0.10	0.35
Ursa Major I	$(1.5 \pm 0.4) \times 10^7$	1024 ± 636	-2.06 ± 0.10	0.46
Leo IV	$(1.4 \pm 1.5) \times 10^6$	151 ± 177	-2.31 ± 0.10	0.15
Coma Berenices	$(1.2 \pm 0.4) \times 10^6$	448 ± 297	-2.00 ± 0.07	0.00
Canes Venatici II	$(2.4 \pm 1.1) \times 10^6$	336 ± 240	-2.31 ± 0.12	0.47
Canes Venatici I	$(2.7 \pm 0.4) \times 10^7$	221 ± 108	-2.09 ± 0.02	0.23
Hercules	$(7.1 \pm 2.6) \times 10^6$	332 ± 221	-2.27 ± 0.07	0.31

[a] UMa II may be a tidally disrupted remnant, which would artificially inflate its mass and mass-to-light ratio.

(half-light) radii rather than King core radii are available in the literature, but we can use the fact that $r_c = 0.64 r_{\rm Plummer}$ to estimate the King radii. The radii and luminosities we have assumed for these calculations are given in the Appendix. Our derived masses for each galaxy are listed in Table 4 and plotted in Figure 10*b*. We note that objects in the bottom left corner of the plot are both the least massive and least luminous known galactic systems.

The ultra-faint Milky Way satellites have masses ranging from just over $10^6\ M_\odot$ (Coma Berenices) up to $2.8 \times 10^7\ M_\odot$ (Canes Venatici I). Not surprisingly, CVn I, which is nearly as bright as previously known dSphs such as Ursa Minor and Draco, has a mass that is similar to those of the original Milky Way dSphs. Combining the measured masses with the absolute magnitudes listed in Table 1, we can calculate *V*-band mass-to-light ratios, which are presented in Table 4. The new dwarfs continue the trend of an anticorrelation between luminosity and M/L that has been known for many years (e.g., Mateo et al. 1993), reaching mass-to-light ratios of $\sim$1000 in *V*-band solar units. Although the uncertainties on the mass-to-light ratios are substantial, owing primarily to the poorly known luminosities of the ultra-faint dwarfs, it is clear that all of these galaxies have quite large mass-to-light ratios. The existence of galaxies with similar properties to these was predicted recently by Ricotti & Gnedin (2005) and Read et al. (2006) but the measured masses seem to be in better agreement with the models of Ricotti & Gnedin (2005).

3.4. *Metallicities*

The mean stellar metallicity of a galaxy reflects the enrichment history of the interstellar medium at the time the stars were formed. We determine the mean metallicity, [Fe/H], for the new dwarf galaxies based on the Ca II triplet equivalent width (§ 2.4). While we can reliably measure equivalent widths for the majority of our target stars, the Rutledge et al. (1997a) empirical calibration that we use to convert to [Fe/H] is valid only for RGB stars. We therefore only include stars brighter than $M_V = +1.5$ and redder than $(g - r) > 0.3$ (to avoid HB stars) in the metallicity analysis. We determine the mean metallicity and metallicity spread using the maximum-likelihood technique described in § 3.2. While the metallicity distributions are not necessarily Gaussian, as the maximum-likelihood calculation assumes, we find that the mean and median of the observed metallicity distributions give similar results. We run the maximum-likelihood algorithm twice, rejecting 3 σ outliers on the second run. The mean metallicities and metallicity spreads are listed in Table 4. We find metallicities ranging from $[Fe/H] = -1.97 \pm 0.15$ for UMa II down to $[Fe/H] = -2.31$ for CVn II and Leo IV. We note that several of our galaxies have mean metallicities equal to those of the most metal-poor globular clusters and lower than those of other dwarf galaxies (Harris 1996; Mateo 1998), making them, along with the Boötes dSph (Muñoz et al. 2006a), the most metal-poor stellar systems known.

A strong correlation exists between the total luminosity of dwarf galaxies in the Local Group and their stellar metallicities (Mateo 1998; Grebel et al. 2003). In comparison, Galactic globular clusters follow no such relationship (Harris 1996). In Figure 11, we show that all but the two faintest of the ultra-low luminosity galaxies follow the luminosity-metallicity relationship defined by the more luminous dSphs. The two galaxies deviating from this relationship are UMa II and Com. These are the nearest as well as the lowest-luminosity objects in our sample, and both galaxies (particularly UMa II) show a variety of evidence suggesting that they are undergoing tidal disruption by the Milky Way. As discussed in § 3.6, we interpret the high metallicities in these two objects as evidence that their formation mass may have been significantly larger than their present mass.

The ultra-low luminosity galaxies extend the luminosity-metallicity relation in the Local Group by an additional 4 mag to $M_V = -4.8$. The location of these seven objects (including Boötes) on the same relationship defined by brighter dSphs is significant. It suggests that the stars formed in these galaxies are connected to the *present* mass of the galaxy and argues against significant tidal stripping, unless the amount of mass stripped from each galaxy approximately preserved the relative ordering of dwarf masses. We also measure significant internal metallicity spreads, $\sigma_{[Fe/H]}$, up to 0.5 dex in several ultra-low luminosity dwarfs, as listed in Table 4. This suggests that stars formed in multiple star formation episodes, rather than a single burst, and firmly distinguishes these faint dwarfs from globular clusters, which do not contain mixed stellar populations. This is clearly the case for Leo T, which shows evidence for multiple stellar populations from its color-magnitude diagram (Irwin et al. 2007). However, a metallicity spread is the only evidence of multiple star formation episodes in the other dwarfs. Further investigation into the detailed abundances of these will provide a much clearer picture of star formation in these low-mass objects.

3.5. *Comments on Individual Galaxies*

Ursa Major II.— UMa II is one of the hardest galaxies to identify based on its signature in the velocity histogram (see Fig. 2*c*), but a clear peak at -117 km s^{-1} emerges once the foreground dwarf stars are screened out by their Na I equivalent widths. Our measured velocity and velocity dispersion are in good agreement with those of Martin et al. (2007). We identify 20 member stars in UMa II out of 236 targeted sources, which represents our lowest detection rate for any of the galaxies. However, this is at least partly a result of our attempt to focus on stars in the outlying clumps noted by Zucker et al. (2006b) rather than the main body of the

this star from the sample then the velocity dispersion of the galaxy would decrease to $2.4^{+0.9}_{-0.7}$ km s^{-1}.

3.6. Tidal Disruption

Two of the dwarfs presented in this paper show at least some evidence for ongoing tidal disruption by the Milky Way. As mentioned in § 3.5, the properties of UMa II and perhaps Com appear to be affected by these interactions.

UMa II is located very close to the Milky Way, second only to Sagittarius (which is the archetype of tidally disrupting dwarfs) among the known dSphs. Zucker et al. (2006b) noted that UMa II appears irregular and that its stars are broken up into several subclumps. Belokurov et al. (2007a) pointed out that the Orphan Stream lies along a great circle intersecting the position of UMa II, and our measured radial velocity of 116.5 ± 1.9 km s^{-1} is in reasonable agreement with the 100 km s^{-1} predicted by Fellhauer et al. (2007) if UMa II is associated with the Orphan Stream. Fellhauer et al. also predict a roughly north-south velocity gradient over several degrees within UMa II. Although our member sample only spans a declination range of 0.6°, we do detect a modest correlation between radial velocity and declination among the member stars (correlation coefficient 0.40), in the same sense as predicted. More significantly, we find strong evidence for a difference in the mean velocity between the eastern and western halves of the galaxy, with the stars on the eastern side having a velocity 8.4 ± 1.4 km s^{-1} larger than those on the western side. It is highly unlikely that a galaxy as small as UMa II would show significant coherent rotation, so this velocity gradient strongly suggests that UMa II is distorted by tidal forces. As noted previously, UMa II is also a clear outlier from the M_V– trend shown in Figure 10*a*. This galaxy therefore either has a mass-to-light ratio several times larger than any other dwarf (Table 4), or its velocity dispersion has been inflated by the tidal field of the Milky Way. Finally, UMa II has a metallicity ~0.5 dex higher than would be expected from the luminosity-metallicity relationship shown in Figure 11. Its metallicity is more appropriate for a system with $M_V \sim -10$ (250 times more luminous than UMa II). Taken together, all of these independent results make a strong case for the imminent tidal disruption of UMa II, and we are not aware of any observational evidence suggesting that UMa II is bound.

Coma Berenices presents an intriguing counterpoint to UMa II. It shares some notable properties with UMa II, including an exceptionally low luminosity ($M_V = -3.7$, compared to $M_V = -3.8$), a location near the Milky Way (44 kpc instead of 32 kpc), and an unexpectedly high stellar metallicity. As with UMa II, we find a modest correlation of velocity with position in the galaxy (correlation coefficient of velocity with right ascension -0.24). Dividing the galaxy in half along the minor axis, we find a mean velocity of 93.3 ± 1.1 km s^{-1} for the northwestern side and a mean velocity of 98.8 ± 0.5 km s^{-1} for the southeastern side. This velocity difference is significant at the 4σ level. As with UMa II, it is not expected that galaxies of this size are rotationally supported, so if this velocity gradient is real it suggests that Coma Berenices, like UMa II, may be distorted by tidal forces. On the other hand, there are no known tidal streams that are plausibly associated with Com, its velocity dispersion is approximately what would be expected given its luminosity, and its stellar distribution is not noticeably more irregular than those of the other ultra-faint dwarfs (there are two bright stars immediately to the north of Com that may be responsible for the apparent distortion of the isopleths in that direction pointed out by Belokurov et al. 2007b). We also note that, with a smaller half-light radius (and larger central density; see § 4.3) than any other Local Group dwarf, Com may be more robust to disruption than some of its counterparts. While the available evidence is suggestive of the possibility that Coma Berenices could be tidally disrupting, the situation is not nearly as clear cut as it is for UMa II. We therefore treat Com as a bound, dark matter dominated object for now, while recognizing that future observations (most importantly, identification of an associated stellar stream) could change this picture.

For the other six galaxies in our sample, we do not detect any statistically significant velocity gradients or other evidence suggesting tidal disruption.

4. DISCUSSION

4.1. The Missing Satellite Problem

Understanding the nature of the ultra-faint dwarf galaxies and determining their impact on the missing satellite problem is one of the key goals of this work. Our observations show that with the likely exception of UMa II (and possibly Coma Berenices as well) the ultra-faint dwarfs seem to be dark matter dominated systems, with masses lower than those of the previously known dSphs and very large mass-to-light ratios. These galaxies are currently the darkest known stellar systems in the universe.

Determining the importance of the effect that the new dwarfs have on the abundance of satellite galaxies around the Milky Way requires having a way to compare observed galaxy properties to the properties of subhalos in *N*-body simulations. The simplest possible approach is to estimate the halo circular velocities of the ultra-faint dwarfs as $v_{\rm circ} = \sqrt{3}\,\sigma$ (Klypin et al. 1999), assuming that the observed dispersions are equivalent to the maximum dispersions reached in each galaxy, and that the stars have negligible orbital anisotropy. Although these assumptions may not be correct in detail, if we use cumulative satellite distributions then the results of this exercise are relatively insensitive to them. The circular velocities of dark matter subhalos in the simulations can be measured robustly, giving us an appropriate point of comparison. We note that a more accurate means of comparing observed dwarfs to simulated subhalos is to use the mass contained within 0.6 kpc, which is better constrained by the observations than the halo circular velocity is (Strigari et al. 2007a); these calculations will be presented in a future paper (L. E. Strigari et al. 2008, in preparation). Using the above approximation, we find that the ultra-faint dwarfs have circular velocities from $v_{\rm circ} = 6$–13 km s^{-1} (for plotting and comparison purposes, we round the circular velocity of Leo IV up to 6 km s^{-1}). Because the fifth data release of the SDSS, where all of the new Milky Way satellites have been discovered, only covers 8000 deg^2 of sky, we must weight each of the new dwarfs by a factor of 5 to account for the additional ultra-faint dwarfs likely to be discovered once the rest of the sky has been similarly surveyed.

We display the cumulative number of Milky Way satellites as a function of circular velocity in Figure 12. We assume Poisson uncertainties on the total number of dwarfs [$\sigma_{\rm tot} = (N_{\rm old} + 5^2 N_{\rm new})^{1/2}$, where $N_{\rm old}$ and $N_{\rm new}$ refer to the previously known and newly discovered dwarf galaxies, respectively]. For comparison, we include the subhalo circular velocity function from the recent Via Lactea simulation, currently the highest resolution (234 million particles) *N*-body simulation of a Milky Way size galaxy (Diemand et al. 2007a, 2007b). This simulation assumes the best-fit WMAP3 yr cosmological parameters: $\Omega_m = 0.238$, $\Omega_\Lambda = 0.762$, $h = 0.73$, $n = 0.951$, and $\sigma_8 = 0.74$ (Spergel et al. 2007). The Via Lactea subhalos include all bound halos located within the virial radius (389 kpc) of the main halo (see also § 4.2). The addition of the new dwarfs, combined with the correction for the sky area that has yet to be observed with sufficient sensitivity, substantially changes the appearance of the substructure problem. The

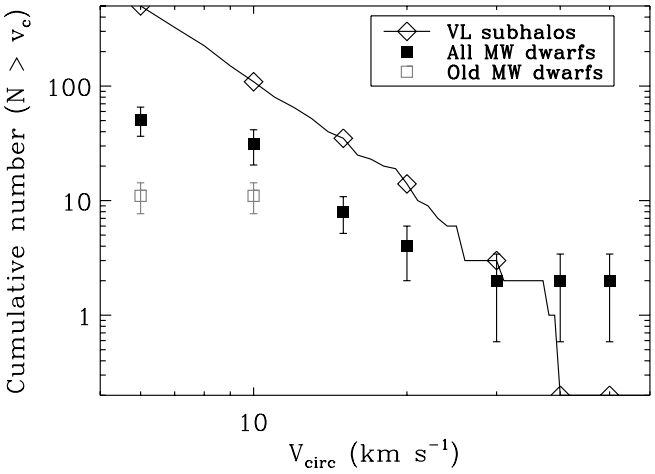

FIG. 12.—Cumulative number of Milky Way satellite galaxies as a function of halo circular velocity. The filled black squares include the new circular velocity estimates from this paper (plus Boötes, but excluding UMa II), as well as all of the previously known Milky Way dwarfs. The open gray squares show the observed distribution without the new ultra-faint dwarfs. We assume Poisson errors on the number count of satellites in each bin (computed independently for the new and old dwarfs), although the true uncertainties may be larger. The solid line with diamonds represents the subhalo abundance within the virial radius of the Via Lactea *N*-body simulation (Diemand et al. 2007a).

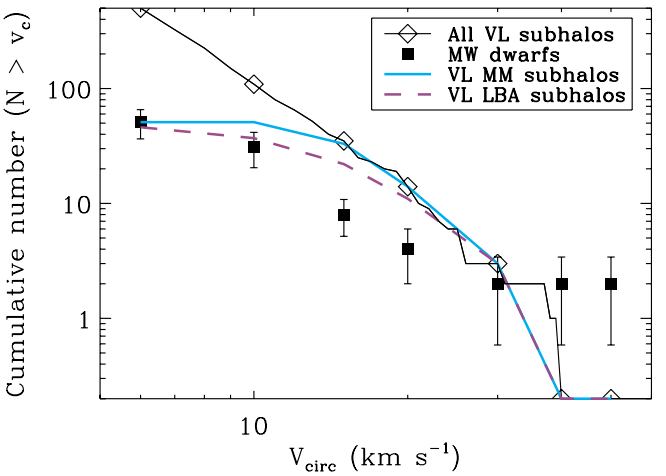

FIG. 13.—Outcome of two proposed solutions to the missing satellite problem. As in Fig. 12, the filled black squares include the new circular velocity estimates from this paper (plus Boötes, but excluding UMa II), as well as all of the previously known Milky Way dwarfs, and the solid line with diamonds represents the subhalo abundance within the virial radius of the Via Lactea *N*-body simulation (Diemand et al. 2007a). The solid cyan curve shows the circular velocity distribution for the 51 most massive Via Lactea subhalos at $z = 0$. The dashed purple curve illustrates the circular velocity distribution for the 51 Via Lactea subhalos that had the largest masses at the time they were accreted by the main halo.

previously known Milky Way satellite galaxies have a nearly flat circular velocity function below $v_{\rm circ} = 15$ km s^{-1}, causing a discrepancy with the predictions that worsens with decreasing mass and reaches well over an order of magnitude below $v_{\rm circ} = 10$ km s^{-1}. With the ultra-faint dwarfs included we now see a rising circular velocity function and a satellite underabundance of a factor of $\sim$4 for halos with masses between $v_{\rm circ} = 10$ and 20 km s^{-1}. At $v_{\rm circ} = 6$ km s^{-1} the discrepancy increases again toward an order of magnitude, but if the current observational census is still incomplete at the faint end, this is the mass range where that would manifest itself. The ultra-faint dwarfs significantly fill in the gap for satellites in the two lowest mass bins, but have masses that are too small to affect the satellite deficit at higher circular velocities.

4.1.1. *Proposed Solutions to the Missing Satellite Problem*

Using these new data, we can test a number of proposed astrophysical solutions to the missing satellite problem. For example, the observed dwarf galaxies could inhabit the most massive subhalos at the present day (Stoehr et al. 2002), the subhalos that collapsed at the highest redshift (Bullock et al. 2000), or the subhalos that were the most massive at the time they were accreted by the Milky Way (Kravtsov et al. 2004). We show the results of these tests in Figures 13 and 14. To compare the observed dwarfs to the most massive (MM) subhalos, we identified the 51 halos (to match the number of Milky Way satellites projected to be found once the remainder of the sky has been surveyed) located within the virial radius that have the largest total masses at the present day in the Via Lactea simulation. The circular velocity function of these subhalos is plotted as the solid cyan curve in Figure 13. Note that because we chose the total number of subhalos to match the total number of Milky Way dwarfs, the agreement between the observed distribution and the cyan curve in the lowest mass bin is trivial. Another possibility is to compare the observed circular velocity function with the circular velocity function of the subhalos that were most massive when they were accreted (Fig. 13, *dashed purple curve*). We selected the largest before accretion (LBA) subhalos from the Via Lactea simulation as the halos located within the virial radius of the main halo at $z = 0$ that had the largest circular velocities at any point in the past. Again, the agreement at the low-mass end is simply a result of our choice of the top 51 subhalos from the simulation.[6] If the observed dwarf galaxies inhabit only the most massive dark matter subhalos around the Milky Way, the shape of the mass function of the most massive subhalos fails to match the shape of the observed mass function. Using the subhalos that were most massive at the time they were accreted

[6] The largest before accretion subsample at the present day (Fig. 13, *dashed purple curve*) actually only has 46 objects with $v_{\rm circ} > 6$ km s^{-1} because five of the subhalos lost so much mass by $z = 0$ that they ended up with even lower present-day circular velocities than are shown in the plot.

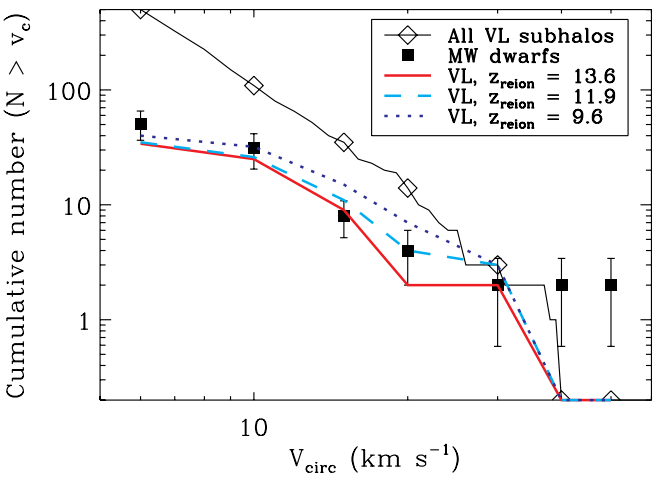

FIG. 14.—Effect of reionization on the missing satellite problem. As in Fig. 12, the filled black squares include the new circular velocity estimates from this paper (plus Boötes, but excluding UMa II), as well as all of the previously known Milky Way dwarfs, and the solid line with diamonds represents the subhalo abundance within the virial radius of the Via Lactea *N*-body simulation (Diemand et al. 2007a). The solid red curve shows the circular velocity distribution for the 51 most massive Via Lactea subhalos at $z = 13.6$, the dashed cyan curve at $z = 11.9$, and the dotted blue curve at $z = 9.6$.

instead of the ones most massive today (i.e., allowing for mass lost by tidal stripping) brings the subhalo mass function slightly closer to the observed one, but there are still a factor of $\sim$3 too few dwarfs in the $v_{\rm circ} = 10$–30 km s^{-1} range.

The final astrophysical solution we consider is that only halos that collapsed prior to reionization were able to form significant numbers of stars (e.g., Bullock et al. 2000; Somerville 2002; Moore et al. 2006). Among the Via Lactea subhalos that are located within the virial radius at $z = 0$, we select the objects with the 51 largest values of $v_{\rm circ}$ at various high redshifts. The results of this test are displayed in Figure 14. The solid red, dashed cyan, and dotted blue curves represent the subhalos that would be selected if $z_{\rm reion} = 13.6$, 11.9, and 9.6, respectively. *If reionization occurred around redshift 9–14, and dwarf galaxy formation was strongly suppressed thereafter, the circular velocity function of Milky Way satellite galaxies approximately matches that of CDM subhalos.* If reionization occurred at $z \lesssim 8$, we again find an underabundance of Milky Way dwarfs with $v_{\rm circ} = 15$–30 km s^{-1} compared to theoretical models, although we note that the individual subhalo $v_{\rm circ}(z)$ histories in the Via Lactea simulation are noisy at high redshift, and the number of objects in these bins is relatively low. We therefore suggest that the observed mass function of Milky Way satellite galaxies constrains reionization to have taken place before $z = 8$, in agreement with the 3 yr *WMAP* results from measurements of the cosmic microwave background ($z_{\rm reion} = 10.9^{+2.7}_{-2.3}$; Page et al. 2007). However, there are a number of caveats to this analysis: (1) the extrapolation of dwarf galaxy abundances from the SDSS DR5 sky coverage to the whole sky must be reasonable; (2) the observed velocity dispersions must provide a reasonable estimate of the halo circular velocities; (3) the primary physical mechanism responsible for suppressing the formation of galaxies in low-mass dark matter halos must be reionization; (4) the cosmology used for the Via Lactea simulation (Diemand et al. 2007a, 2007b)—particularly the low value of σ_8—must be a good match to the cosmology of our universe; and (5) the main halo simulated in Via Lactea must be a reasonable representation of the Milky Way. We also note that while *WMAP* and most other observational probes are sensitive to the mean reionization history of the universe, the dwarf galaxies observed in the study are sensitive primarily to the reionization history *of the Local Group*. If reionization was indeed responsible for the low abundance of Galactic satellites, then the Milky Way and/or M31 must have been undergoing vigorous enough star formation to ionize the intergalactic medium of the Local Group at $z > 8$.

4.1.2. *Observational Incompleteness and the Comparison Radius in Simulations*

One of the important assumptions involved in our analysis in §§ 4.1 and 4.1.1 is the choice of the radius in the simulations out to which satellites should be counted. In the ideal case, this radius should be the virial radius, as we have used, but in reality the comparison between observations and simulations is only meaningful in the regime where the observations are complete.

The observational census for Milky Way satellite galaxies similar to the brighter dwarf spheroidals ($M_V \lesssim -9$) should be largely complete by now; the last Milky Way satellite to be discovered in this luminosity range was Sagittarius (Ibata et al. 1994). Recent searches of Palomar Sky Survey data, which are sensitive to such galaxies anywhere within the Local Group, have not detected additional dwarfs (Whiting et al. 2007; Simon & Blitz 2002). The distribution of Milky Way dwarf galaxies as a function of Galactic latitude suggests that additional relatively bright dwarfs remain to be discovered at low latitudes, where extinction and foreground confusion are serious problems. The expected number of such objects if they are distributed uniformly around the Galaxy is $\sim$4 (Mateo 1998; Willman et al. 2004), which does not appear to be enough to significantly affect the missing satellite problem.

Very recently, Koposov et al. (2007) have analyzed the detectability of faint Milky Way satellites in the SDSS DR5 data. They find that extremely low-luminosity objects ($M_V \lesssim -5$) may be missed by SDSS searches if they are located at relatively large distances ($d \gtrsim 100$ kpc), as the horizontal branch and MSTO stars that their detection relies on become too faint to be reliably detected in the SDSS. Galaxies with even lower surface brightnesses than the known dwarfs ($\mu_V \gtrsim 30$ mag arcsec^{-2}), if they exist, are also likely to have escaped detection. However, if there is a correlation between surface brightness and distance from the host galaxy (e.g., McConnachie & Irwin 2006) or density and distance (as our data and Mayer et al. [2001b] suggest), there may not be significant numbers of ultra-faint dwarfs at large distances. For more luminous dwarfs and those with higher central surface brightnesses, the current sample of Milky Way satellites should be reasonably complete. The Koposov et al. (2007) luminosity function of Milky Way satellite galaxies predicts that there are a total of 57 dwarf galaxies within 280 kpc of the Milky Way over the whole sky, and a similar number within 420 kpc. Thus, our much simpler estimates of 46 ± 14 dwarf galaxies within 250 kpc and 51 ± 15 within 420 kpc from § 4.1 appear to be well justified.

Incompleteness may still be a significant problem at the extreme faint end of the luminosity function, as the recent discovery of Boötes II reveals (Walsh et al. 2007). Our results suggest that satellites in this luminosity range are not gravitationally bound dwarf galaxies. If these objects are tidally disrupted dwarfs, then they should still contribute to the Milky Way satellite census, but if they are simply multiple fragments from larger objects (for example, if there is a physical connection between Boötes and Boötes II) or unusual globular clusters then they do not correspond to dark matter subhalos in the CDM simulations. Until surveys are more complete at faint magnitudes and some kinematic information is available for this class of objects, their effect on the missing satellite problem is not clear.

In case there are undiscovered ultra-faint Milky Way dwarfs beyond $d = 250$ kpc, we repeated our analysis of § 4.1 using subhalos within 250 kpc from the main halo in the Via Lactea simulation (and discarding Leo T from the observed sample because it is beyond this radius). This smaller radius reduces the overall number of satellite subhalos by $\sim$30%, not enough to significantly change our conclusions. Limiting the comparison to this radius shifts the preferred range of reionization redshifts slightly lower, but also lessens our leverage on determining the redshift of reionization.

4.2. *The Constant Halo Mass Hypothesis*

Mateo et al. (1993) was the first to point out that observations of the dSphs known at that time suggested that they were all embedded within dark matter halos of mass $\sim 3 \times 10^7\, M_\odot$, independent of luminosity. In Figure 15 we display an updated version of what has become popularly known as the "Mateo" plot, showing the mass-to-light ratios of all of the Local Group dSphs with measured kinematics as a function of absolute magnitude. As seen previously by Mateo et al. (1993), Mateo (1998), and Gilmore et al. (2007), all of the galaxies observed prior to this work are approximately consistent with the picture proposed by Mateo et al. (1993). The results change, however, when the ultra-faint Milky Way satellites are added. Although the brightest of the ultra-faint dwarfs still lie within the same range of halo mass as their more luminous counterparts, the fainter objects (Hercules, Leo IV, CVn II, and Coma Berenices) are located well below

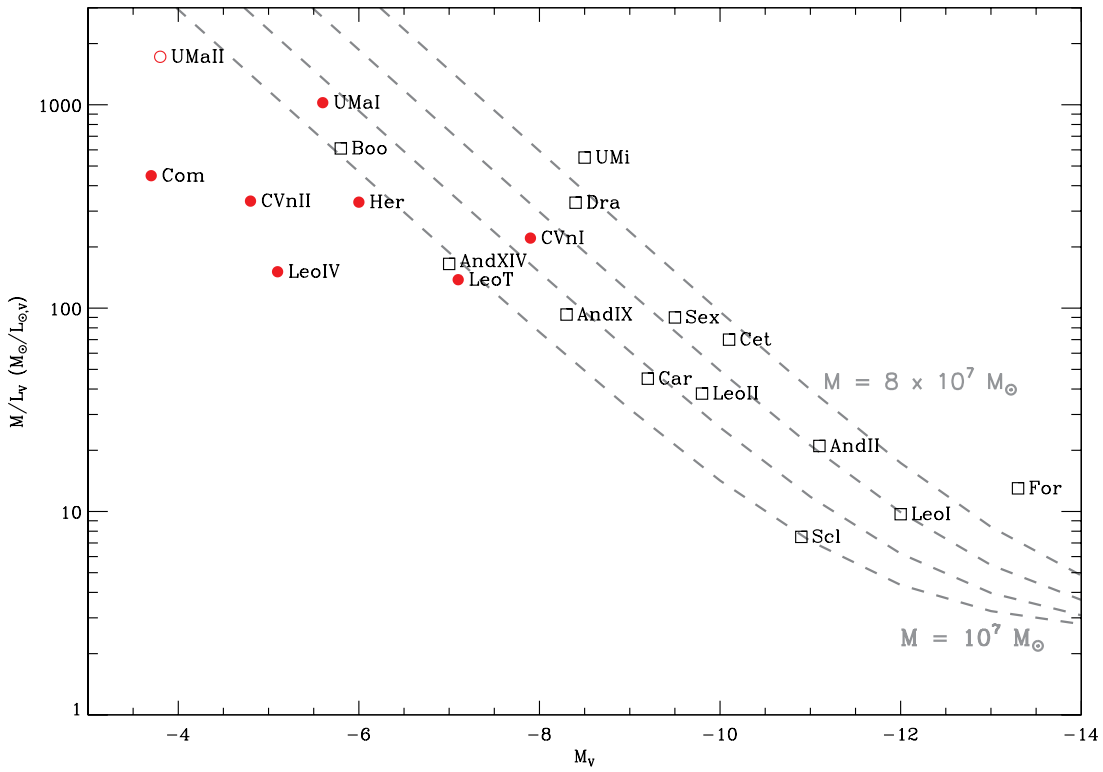

FIG. 15.—Total mass-to-light ratios (in solar units) as a function of absolute magnitude for Local Group dwarf spheroidals. The red symbols represent the ultra-faint dwarfs from this paper (including Leo T, which is not really a dSph, and UMa II, which may be tidally disrupted, as an open red circle at the upper left). The open black squares represent all of the dSphs with previously published kinematic data, including satellites of M31 as well as the Milky Way. The dashed gray lines are curves of constant dark matter halo mass (1, 2, 4, and $8 \times 10^7\ M_\odot$, from bottom to top), assuming a stellar mass-to-light ratio of $2.5\ M_\odot/L_{\odot,V}$. For the previously known Milky Way dwarfs, we recomputed luminosities from Irwin & Hatzidimitriou (1995) using the most up-to-date distance measurements, and then adjusted the mass-to-light ratios from the literature accordingly. References for distance measurements are Fornax: Saviane et al. (2000), Mackey & Gilmore (2003), Gullieuszik et al. (2007); Leo I: Bellazzini et al. (2004); Sculptor: Mateo (1998); Leo II: Bellazzini et al. (2005); Sextans: Lee et al. (2003); Carina: Dall'Ora et al. (2003); Ursa Minor: Mighell & Burke (1999); and Draco: Bonanos et al. (2004). References for M/L measurements are Fornax: Walker et al. (2006a); Leo I: Sohn et al. (2007), Koch et al. (2007b); Sculptor: Westfall et al. (2006); Leo II: Koch et al. (2007a); Sextans: Walker et al. (2006b); Carina: Muñoz et al. (2006b); Ursa Minor: Wu (2007); Draco: Łokas et al. (2005); And II: Côté et al. (1999); Cetus: Lewis et al. (2007); And IX: Chapman et al. (2005); And XIV: Majewski et al. (2007); and Boötes: Muñoz et al. (2006a).

the extrapolated trend. These galaxies have much lower halo masses, and hence their mass-to-light ratios are significantly smaller than what would be expected if they too were embedded in $\sim 3 \times 10^7\ M_\odot$ halos. Combining the new and old dwarfs, it appears that there are two distinct regimes: the brighter dwarfs ($M_V < -9$) all have similar-mass dark matter halos, but for the fainter dwarfs ($M_V > -9$) M/L saturates at a value of 200–1000 and the halo mass declines as luminosity decreases (see Fig. 10*b*). It therefore appears that the ultra-faint dwarfs *do not* occupy halos as massive as those of the "normal" dSphs; if there is a minimum halo mass for dwarf galaxies, it is not clear that the observations have yet reached it.

4.3. *Central Dark Matter Densities in the Ultra-faint Dwarfs*

The observed velocity dispersions and radii of the new dwarfs constrain their densities as well as their masses and mass-to-light ratios. Because these galaxies are highly dark matter dominated, the overall densities we derive are essentially equal to the density of the dark matter halo of each object. Following Mateo et al. (1991), we can approximate the central density as

$$166\sigma^2\eta/r_c^2, \tag{4}$$

where η is a numerical parameter that works out to 1 for plausible density profiles. The central densities of the new dwarfs range from $\sim 0.08\ M_\odot\ \mathrm{pc}^{-3}$ for CVn I and Hercules up to $\sim 2.1\ M_\odot\ \mathrm{pc}^{-3}$ for the faintest galaxy, Coma Berenices. Alternatively, we can calculate mean densities from the total masses given in Table 4 and the core radii. To compare with the mean densities of the previously known Milky Way dSphs tabulated by Gilmore et al. (2007), we assume that the extent of the new dwarfs is ~ 2 King core radii. Again, Coma Berenices is the densest object, with a mean density of $0.52\ M_\odot\ \mathrm{pc}^{-3}$ ($=20\ \mathrm{GeV}/c^2\ \mathrm{cm}^{-3}$), almost a factor of 5 higher than any of the previously known dSphs. This substantially raises the limiting mass density of $\sim 5\ \mathrm{GeV}/c^2\ \mathrm{cm}^{-3}$ identified by Gilmore et al. (2007) and suggests that there may not be a true physical ceiling on the densities of dwarf galaxies (as opposed to an observational ceiling) at all. However, if Com is in the process of tidal disruption, as our observations hint, then the highest dark matter densities in our sample occur in Leo T and CVn II and are only modestly above the density limit of Gilmore et al. (2007).

4.4. *Phase-Space Density Constraints from the Ultra-faint Dwarfs*

Hogan & Dalcanton (2000) introduced the parameter $Q \equiv \rho/\sigma^3$ as an estimate of the coarse-grained phase-space density of the dark matter in galaxy halos. As discussed by Hogan & Dalcanton (2000), Dalcanton & Hogan (2001), and Strigari et al. (2006), Liouville's theorem implies that observed values of Q set a hard lower limit on the original phase-space density of the dark matter. By finding the systems with the largest observed values of Q, we can therefore constrain the properties of dark matter and potentially rule out classes of dark matter candidates. Observations of low-mass spiral galaxies by Simon et al. (2005) yield lower

TABLE 5
PHYSICAL AND PHASE-SPACE DENSITIES

Galaxy	ρ_0 ($M_\odot$ pc^{-3})	$\bar{\rho}$ ($M_\odot$ pc^{-3})	Q [$M_\odot$ pc^{-3} (km s^{-1})$^{-3}$]
Ursa Major II[a]	1.13 ± 0.60	0.27 ± 0.18	$(3.7 \pm 3.1) \times 10^{-3}$
Leo T	0.79 ± 0.36	0.19 ± 0.10	$(1.9 \pm 1.5) \times 10^{-3}$
Ursa Major I	0.25 ± 0.08	0.06 ± 0.02	$(5.6 \pm 2.9) \times 10^{-4}$
Leo IV	0.19 ± 0.20	0.05 ± 0.05	$(5.3 \pm 9.9) \times 10^{-3}$
Coma Berenices	2.09 ± 0.86	0.52 ± 0.24	$(2.2 \pm 1.4) \times 10^{-2}$
Canes Venatici II	0.49 ± 0.25	0.12 ± 0.07	$(5.1 \pm 4.1) \times 10^{-3}$
Canes Venatici I	0.08 ± 0.02	0.02 ± 0.01	$(1.7 \pm 0.5) \times 10^{-4}$
Hercules	0.10 ± 0.04	0.02 ± 0.01	$(7.7 \pm 5.2) \times 10^{-4}$

[a] UMa II may be a tidally disrupted remnant, which would artificially inflate its density.

limits of $\sim 10^{-6}\ M_\odot$ pc^{-3} (km s^{-1})$^{-3}$ on Q (Strigari et al. 2006; G. Martinez et al. 2008, in preparation), but those are less restrictive constraints than are provided by the Lyα forest. Q values for the ultra-faint dwarfs are listed in Table 5. These values are calculated under the assumption that the velocity dispersion of the dark matter (which is what Q actually depends on) is equal to the velocity dispersion of the stars. Our observations show that most of the ultra-faint dwarfs greatly exceed the phase-space density constraint from the Lyα forest, reaching a maximum of $Q = 2.2 \times 10^{-2}\ M_\odot$ pc^{-3} (km s^{-1})$^{-3}$ in Coma Berenices. Even if the derived Q of Com has been affected by tidal disruption, all of the galaxies except UMa I, CVn I, and Hercules have Q values $\gtrsim 10^{-3}\ M_\odot$ pc^{-3} (km s^{-1})$^{-3}$, 2 orders of magnitude better than the Lyα forest constraint and about an order of magnitude improvement compared to the previously known dSphs. In fact, the dark matter velocity dispersion is expected to be larger than the stellar velocity dispersion, so the Q values we derive are upper limits on the true Q values for these galaxies. Nevertheless, these Q values will further restrict the allowed parameter space for warm dark matter particles, and may have an impact on the meta-CDM scenario proposed by Strigari et al. (2007b).

5. SUMMARY AND CONCLUSIONS

We have obtained Keck DEIMOS spectra of significant samples of stars in eight of the new, ultra-faint Milky Way satellite galaxies recently discovered in the Sloan Digital Sky Survey. Using a large spectroscopic data set of radial velocity standard stars observed with DEIMOS, repeat DEIMOS measurements of stars in dwarf spheroidals and globular clusters, and DEIMOS and HIRES spectra of the same stars, we demonstrated that both our velocity measurements and our derived uncertainties are accurate. We then measured the velocities of 18–214 stars in each galaxy, with typical uncertainties of ~ 3.4 km s^{-1}.

From our measurements of individual stellar velocities, we calculated velocity dispersions for each of the ultra-faint dwarfs. The velocity dispersions, which are listed in Table 3, range from 3.3 ± 1.7 km s^{-1} for Leo IV up to 7.6 ± 0.4 km s^{-1} for CVn I, and we showed that the velocity dispersions are correlated with luminosity (inversely correlated with absolute magnitude). Under a set of simple assumptions, we calculated the total masses of the ultra-faint dwarfs, finding that these objects are the lowest-mass galaxies currently known. From the equivalent widths of the Ca triplet absorption lines we measured the metallicities of the RGB stars in the new dwarfs and derived mean metallicities ranging from [Fe/H] $= -2.0$ to [Fe/H] $= -2.3$; several of these galaxies are the most metal-poor stellar systems yet discovered.

We summarize our primary conclusions from this study as follows:

1. The ultra-faint Milky Way satellites are dark matter dominated dwarf galaxies with lower masses than any other known galaxies.

2. The only clear exception among the eight galaxies we observed, as well as those previously observed by others, is Ursa Major II. Based on its clumpy appearance (Zucker et al. 2006b), small galactocentric distance (Zucker et al. 2006b), associated tidal stream (Fellhauer et al. 2007) (§ 3.5), inflated velocity dispersion (§ 3.2), unusually high metallicity (§ 3.4), and possible velocity gradient (§ 3.5), we conclude that UMa II is in the late stages of tidal disruption. The other dwarf with $M_V \gtrsim -4$, Coma Berenices, has a similarly high metallicity that indicates it may have suffered substantial tidal stripping as well. Because Com lacks most of the other supporting evidence for tidal disruption, we assume for now that it is still a bound, dark matter dominated dwarf, although we recognize that future observations may show otherwise. Based on these results, we suggest that $M_V \approx -4$ ($3.4 \times 10^3\ L_\odot$) is the lower limit to the luminosity of gravitationally bound dwarf galaxies. We therefore predict that objects such as Willman 1, Segue 1, and Boötes II will prove to be tidally disrupted remnants.

3. The six ultra-faint dwarfs with $M_V \lesssim -4$ follow the luminosity-metallicity relationship established by the more luminous Local Group dwarfs, and extend the relation by ~ 2 orders of magnitude in luminosity. The faintest dwarfs, UMa II and Com, are both outliers from this relationship, with metallicities more than 0.5 dex too large for their luminosities (or conversely, luminosities that are more than 2 orders of magnitude too small for their metallicities). We detect metallicity spreads of up to 0.5 dex in several objects, suggesting multiple star formation epochs.

4. The total mass-to-light ratios of the ultra-faint dwarfs reach as high as 1000 $M_\odot/L_{\odot,V}$ (UMa I). While the brighter galaxies ($M_V \lesssim -9$) have mass-to-light ratios consistent with the hypothesis that all dwarf spheroidals are embedded within dark matter halos of the same mass, the fainter galaxies depart from this trend in the sense that their mass-to-light ratios are too low (i.e., they have lower masses). We therefore suggest that the minimum *mass* for dwarf galaxies (as opposed to the minimum luminosity mentioned earlier), if there is one, may not have been reached yet.

5. The ultra-faint Milky Way satellites, after correcting for the sky area not covered by DR5 of the Sloan survey, substantially increase the abundance of dwarf galaxies with very low masses ($v_{\rm circ} \leq 15$ km s^{-1}), thereby reducing the satellite deficit compared to CDM simulations to a factor of ~ 4. Proposals to remedy the missing satellite problem by placing the observed dwarf galaxies in the most massive dark matter subhalos (at the present day) around the Milky Way or in the subhalos that were most massive at the time they were accreted by the Milky Way do not reproduce the observed shape of the circular velocity function. If we assume instead that only the halos that acquired a significant amount of mass ($v_{\rm circ} \gtrsim 8$ km s^{-1}, varying somewhat with $z_{\rm reion}$) before the redshift of reionization were able to form stars, then the subhalos from the Via Lactea simulation (Diemand et al. 2007a, 2007b) approximately match both the total number of Milky Way dwarfs and the shape of the circular velocity function.

6. The central dark matter densities of the ultra-faint dwarfs are as high as 2.1 $M_\odot$ pc^{-3} (0.8 $M_\odot$ pc^{-3} if Coma Berenices is tidally disrupting), significantly larger than those of the previously known dwarf spheroidals. The phase-space densities are also higher than those of other astrophysical systems [$Q > 10^{-3}\ M_\odot$ pc^{-3} (km s^{-1})$^{-3}$], which will place significant limits on non-CDM dark matter models.

Data presented herein were obtained at the W. M. Keck Observatory, which is operated as a scientific partnership among the California Institute of Technology, the University of California, and the National Aeronautics and Space Administration. The observatory was made possible by the generous financial support of the W. M. Keck Foundation. The authors wish to recognize and acknowledge the very significant cultural role and reverence that the summit of Mauna Kea has always had within the indigenous Hawaiian community. We are most fortunate to have the opportunity to conduct observations from this mountain. J. D. S. gratefully acknowledges the support of a Millikan Fellowship provided by Caltech and M. G. acknowledges support from a Plaskett Research Fellowship at the Herzberg Institute of Astrophysics of the National Research Council of Canada. We thank George Djorgovski, Vasily Belokurov, Leo Blitz, James Bullock, Judy Cohen, Pat Côté, Jürg Diemand, Gerry Gilmore, Raja Guhathakurta, Nicolas Martin, Emma Ryan-Weber, Wal Sargent, Peter Stetson, Louie Strigari, Beth Willman, and Dan Zucker for helpful conversations, and we acknowledge the useful suggestions of the anonymous referee. We also thank Michael Cooper and the DEEP2 team for their hard work on the DEIMOS data reduction pipeline. The analysis pipeline used to reduce the DEIMOS data was developed at UC Berkeley with support from NSF grant AST-0071048. This research has made use of NASA's Astrophysics Data System Bibliographic Services, the NASA/IPAC Extragalactic Database (NED), which is operated by the Jet Propulsion Laboratory, California Institute of Technology, under contract with the National Aeronautics and Space Administration, and the SIMBAD database, operated at CDS, Strasbourg, France.

Facilities: Keck:II (DEIMOS)

APPENDIX

COLLECTING UNIFORM DATA FOR THE ULTRA-FAINT DWARF GALAXIES

The new ultra-faint dwarf galaxies have been discovered by a number of different authors, which means that their properties have not all been determined in a uniform manner. In order to calculate masses and mass-to-light ratios as consistently as possible for each galaxy, and to facilitate future studies of these objects, in this Appendix we collect the currently available data on all 12 of the new Milky Way satellites (see Table 6).

With the exception of Willman 1 and Boötes II, we use the absolute magnitudes and radii determined by the Cambridge group (references given in Tables 1 and 6) from the SDSS data. This includes the revised absolute magnitude of $M_V = -5.5$ for UMa I reported in Belokurov et al. (2006), which differs substantially from the original value of $M_V = -6.75$ estimated by Willman et al. (2005a), although the uncertainties on both numbers are admittedly large. Note that our improved distance for UMa I of 106 kpc (compared to the previously reported 100 kpc) requires a corresponding change in the absolute magnitude to $M_V = -5.6$. The Belokurov et al. magnitude for UMa I is not accompanied by an uncertainty; by analogy to the other galaxies of similar luminosity we assume an uncertainty of 0.6 mag. Belokurov et al. have also remeasured the radius of UMa I in the same manner as they did for the other Milky Way galaxies, finding a Plummer radius of 10′ (D. Zucker & V. Belokurov 2007, private communication).

UMa II is described in the discovery paper only as having an angular extent of $\sim 0.5^\circ \times 0.25^\circ$ and a half-light radius of approximately 120 pc (Zucker et al. 2006b). Similarly to UMa I, the authors have refit the light profile using the same method as they did for the other new dwarfs and measured a half-light radius of 13.6′ (D. Zucker & V. Belokurov 2007, private communication). Note that unlike the Plummer radii we use for the other dwarfs, this radius is the mean of the Plummer radius and the exponential scale radius; in most cases the two radii are very similar.

Boötes II does not have a published distance uncertainty, so given the angular proximity to Boötes and the apparently identical distance moduli, we assume the same distance uncertainty for Boötes II as Belokurov et al. (2006) derived for Boötes.

Most of the new discoveries do not have published uncertainties for their Plummer radius fits. For these objects, we assume an uncertainty of 6% (the uncertainty given for CVn I) on the angular radius for the purposes of calculating the uncertainty on the corresponding physical radius.

TABLE 6
Parameters of the Ultra-faint Milky Way Satellites

Galaxy	M_V	Distance (kpc)	$r_{\rm Plummer}$ (arcmin)	$r_{\rm Plummer}$ (pc)	References
Ursa Major II	-3.8 ± 0.6	32^{+5}_{-4}	13.6	127 ± 21	1, 2
Leo T	-7.1 ± 0.3	417^{+20}_{-19}	1.4	170 ± 15	3
Ursa Major I	-5.6 ± 0.6	106^{+9}_{-8}	10.0	308 ± 32	2, 4, 5
Leo IV	-5.1 ± 0.6	158^{+15}_{-14}	3.3	152 ± 17	6
Coma Berenices	-3.7 ± 0.6	44 ± 4	5.0	64 ± 7	6
Canes Venatici II	-4.8 ± 0.6	151^{+15}_{-13}	3.0	132 ± 16	6
Canes Venatici I	-7.9 ± 0.5	224^{+22}_{-20}	8.5 ± 0.5	554 ± 63	7
Hercules	-6.0 ± 0.6	138^{+13}_{-12}	8.0	321 ± 36	6
Segue 1	-3.0 ± 0.6	23 ± 2	4.5	30 ± 3	6
Willman 1	-2.5 ± 1.0	38 ± 7	1.9 ± 0.3	21 ± 5	8
Boötes II	-3.1 ± 1.1	60 ± 6	4.1 ± 1.6	72 ± 28	9
Boötes	-5.8 ± 0.5	60 ± 6	13.0 ± 0.7	227 ± 26	3

References.—(1) Zucker et al. 2006b; (2) D. Zucker & V. Belokurov 2007, private communication; (3) Irwin et al. 2007; (4) Belokurov et al. 2006; (5) this work; (6) Belokurov et al. 2007b; (7) Zucker et al. 2006a; (8) Willman et al. 2006; (9) Walsh et al. 2007.

REFERENCES

Adelman-McCarthy, J., et al. 2007, ApJS, 172, 634
Bellazzini, M., Gennari, N., & Ferraro, F. R. 2005, MNRAS, 360, 185
Bellazzini, M., Gennari, N., Ferraro, F. R., & Sollima, A. 2004, MNRAS, 354, 708
Belokurov, V., et al. 2006, ApJ, 647, L111
———. 2007a, ApJ, 658, 337
———. 2007b, ApJ, 654, 897
Benson, A. J., Frenk, C. S., Lacey, C. G., Baugh, C. M., & Cole, S. 2002, MNRAS, 333, 177
Blanton, M. R., & Roweis, S. 2007, AJ, 133, 734
Blanton, M. R., et al. 2005, AJ, 129, 2562
Bode, P., Ostriker, J. P., & Turok, N. 2001, ApJ, 556, 93
Bonanos, A. Z., Stanek, K. Z., Szentgyorgyi, A. H., Sasselov, D. D., & Bakos, G. Á. 2004, AJ, 127, 861
Bullock, J. S., Kravtsov, A. V., & Weinberg, D. H. 2000, ApJ, 539, 517
Carretta, E., & Gratton, R. G. 1997, A&AS, 121, 95
Chapman, S. C., Ibata, R., Lewis, G. F., Ferguson, A. M. N., Irwin, M., McConnachie, A., & Tanvir, N. 2005, ApJ, 632, L87
Clem, J. L. 2005, Ph.D. thesis, Univ. Victoria
Coleman, M. G., et al. 2007, ApJ, 668, L43
Colín, P., Avila-Reese, V., & Valenzuela, O. 2000, ApJ, 542, 622
Côté, P., Mateo, M., Olszewski, E. W., & Cook, K. H. 1999, ApJ, 526, 147
Dalcanton, J. J., & Hogan, C. J. 2001, ApJ, 561, 35
Dall'Ora, M., et al. 2003, AJ, 126, 197
Diemand, J., Kuhlen, M., & Madau, P. 2007a, ApJ, 657, 262
———. 2007b, ApJ, 667, 859
Faber, S. M., et al. 2003, Proc. SPIE, 4841, 1657
Fellhauer, M., et al. 2007, MNRAS, 375, 1171
Gilbert, K. M., et al. 2006, ApJ, 652, 1188
Gilmore, G., Wilkinson, M. I., Wyse, R. F. G., Kleyna, J. T., Koch, A., Evans, N. W., & Grebel, E. K. 2007, ApJ, 663, 948
Girardi, L., Grebel, E. K., Odenkirchen, M., & Chiosi, C. 2004, A&A, 422, 205
Grebel, E. K., Gallagher, J. S., & Harbeck, D. 2003, AJ, 125, 1926
Grillmair, C. J. 2006, ApJ, 645, L37
Guhathakurta, P., et al. 2006, AJ, 131, 2497
Gullieuszik, M., Held, E. V., Rizzi, L., Saviane, I., Momany, Y., & Ortolani, S. 2007, A&A, 467, 1025
Harris, W. E. 1996, AJ, 112, 1487
Hogan, C. J., & Dalcanton, J. J. 2000, Phys. Rev. D, 62, 063511
Ibata, R., Chapman, S., Irwin, M., Lewis, G., & Martin, N. 2006, MNRAS, 373, L70
Ibata, R., Martin, N. F., Irwin, M., Chapman, S., Ferguson, A. M. N., Lewis, G. F., & McConnachie, A. W. 2007, ApJ, submitted (arXiv: 0704.1318)
Ibata, R. A., Gilmore, G., & Irwin, M. J. 1994, Nature, 370, 194
Illingworth, G. 1976, ApJ, 204, 73
Irwin, M., & Hatzidimitriou, D. 1995, MNRAS, 277, 1354
Irwin, M. J., et al. 2007, ApJ, 656, L13
Kamionkowski, M., & Liddle, A. R. 2000, Phys. Rev. Lett., 84, 4525
Kauffmann, G., White, S. D. M., & Guiderdoni, B. 1993, MNRAS, 264, 201
King, I. 1962, AJ, 67, 471
Kleyna, J., Geller, M., Kenyon, S., & Kurtz, M. 1999, AJ, 117, 1275
Kleyna, J. T., Wilkinson, M. I., Evans, N. W., & Gilmore, G. 2005, ApJ, 630, L141
Klypin, A., Kravtsov, A. V., Valenzuela, O., & Prada, F. 1999, ApJ, 522, 82
Koch, A., Grebel, E. K., Wyse, R. F. G., Kleyna, J. T., Wilkinson, M. I., Harbeck, D. R., Gilmore, G. F., & Evans, N. W. 2006, AJ, 131, 895
Koch, A., Kleyna, J. T., Wilkinson, M. I., Grebel, E. K., Gilmore, G. F., Evans, N. W., Wyse, R. F. G., & Harbeck, D. R. 2007a, AJ, 134, 566
Koch, A., Wilkinson, M. I., Kleyna, J. T., Gilmore, G. F., Grebel, E. K., Mackey, A. D., Evans, N. W., & Wyse, R. F. G. 2007b, ApJ, 657, 241
Koposov, S., et al. 2007, ApJ, submitted (arXiv: 0706.2687)
Kravtsov, A. V., Gnedin, O. Y., & Klypin, A. A. 2004, ApJ, 609, 482
Lee, M. G., et al. 2003, AJ, 126, 2840
Lewis, G. F., Ibata, R. A., Chapman, S. C., McConnachie, A., Irwin, M. J., Tolstoy, E., & Tanvir, N. R. 2007, MNRAS, 375, 1364
Łokas, E. L., Mamon, G. A., & Prada, F. 2005, MNRAS, 363, 918
Mackey, A. D., & Gilmore, G. F. 2003, MNRAS, 345, 747
Majewski, S. R., et al. 2007, ApJ, submitted (astro-ph/0702635)
Marcolini, A., D'Ercole, A., Brighenti, F., & Recchi, S. 2006, MNRAS, 371, 643
Martin, N. F., Ibata, R. A., Chapman, S., Irwin, M., & Lewis, G. F. 2007, MNRAS, 380, 281
Martin, N. F., Ibata, R. A., Irwin, M. J., Chapman, S., Lewis, G. F., Ferguson, A. M. N., Tanvir, N., & McConnachie, A. W. 2006, MNRAS, 371, 1983
Mateo, M., Olszewski, E., Welch, D. L., Fischer, P., & Kunkel, W. 1991, AJ, 102, 914
Mateo, M., Olszewski, E. W., Pryor, C., Welch, D. L., & Fischer, P. 1993, AJ, 105, 510
Mateo, M. L. 1998, ARA&A, 36, 435
Mayer, L., Governato, F., Colpi, M., Moore, B., Quinn, T., Wadsley, J., Stadel, J., & Lake, G. 2001a, ApJ, 547, L123
———. 2001b, ApJ, 559, 754
McConnachie, A. W., & Irwin, M. J. 2006, MNRAS, 365, 1263
Mighell, K. J., & Burke, C. J. 1999, AJ, 118, 366
Moore, B., Diemand, J., Madau, P., Zemp, M., & Stadel, J. 2006, MNRAS, 368, 563
Moore, B., Ghigna, S., Governato, F., Lake, G., Quinn, T., Stadel, J., & Tozzi, P. 1999, ApJ, 524, L19
Muñoz, R. R., Carlin, J. L., Frinchaboy, P. M., Nidever, D. L., Majewski, S. R., & Patterson, R. J. 2006a, ApJ, 650, L51
Muñoz, R. R., et al. 2006b, ApJ, 649, 201
Olszewski, E. W., Pryor, C., & Armandroff, T. E. 1996, AJ, 111, 750
Page, L., et al. 2007, ApJS, 170, 335
Pryor, C., & Meylan, G. 1993, ASP Conf. Ser. 50, Structure and Dynamics of Globular Clusters, ed. S.G. Djorgovski & G. Meylan (San Francisco: ASP), 357
Read, J. I., Pontzen, A. P., & Viel, M. 2006, MNRAS, 371, 885
Ricotti, M., & Gnedin, N. Y. 2005, ApJ, 629, 259
Rutledge, G. A., Hesser, J. E., & Stetson, P. B. 1997a, PASP, 109, 907
Rutledge, G. A., Hesser, J. E., Stetson, P. B., Mateo, M., Simard, L., Bolte, M., Friel, E. D., & Copin, Y. 1997b, PASP, 109, 883
Ryan-Weber, E. V., Begum, A., Oosterloo, T., Pal, S. Irwin, M. J., Belokurov, V., Evans, N. W. & Zucker, D. B. 2007, MNRAS, submitted
Sakamoto, T., & Hasegawa, T. 2006, ApJ, 653, L29
Saviane, I., Held, E. V., & Bertelli, G. 2000, A&A, 355, 56
Schiavon, R. P., Barbuy, B., Rossi, S. C. F., & Milone, A. 1997, ApJ, 479, 902
Schlegel, D. J., Finkbeiner, D. P., & Davis, M. 1998, ApJ, 500, 525
Simon, J. D., & Blitz, L. 2002, ApJ, 574, 726
Simon, J. D., Bolatto, A. D., Leroy, A., Blitz, L., & Gates, E. L. 2005, ApJ, 621, 757
Sohn, S. T., et al. 2007, ApJ, 663, 960
Somerville, R. S. 2002, ApJ, 572, L23
Spergel, D. N., et al. 2007, ApJS, 170, 377
Spinrad, H., & Taylor, B. J. 1971, ApJS, 22, 445
Stoehr, F., White, S. D. M., Tormen, G., & Springel, V. 2002, MNRAS, 335, L84
Strigari, L. E., Bullock, J. S., Kaplinghat, M., Diemand, J., Kuhlen, M., & Madau, P. 2007a, ApJ, 669, 676
Strigari, L. E., Bullock, J. S., Kaplinghat, M., Kravtsov, A. V., Gnedin, O. Y., Abazajian, K., & Klypin, A. A. 2006, ApJ, 652, 306
Strigari, L. E., Kaplinghat, M., & Bullock, J. S. 2007b, Phys. Rev. D, 75, 061303
Walker, M. G., Mateo, M., Olszewski, E. W., Bernstein, R., Wang, X., & Woodroofe, M. 2006a, AJ, 131, 2114
Walker, M. G., Mateo, M., Olszewski, E. W., Pal, J. K., Sen, B., & Woodroofe, M. 2006b, ApJ, 642, L41
Walsh, S. M., Jerjen, H., & Willman, B. 2007, ApJ, 662, L83
Westfall, K. B., Majewski, S. R., Ostheimer, J. C., Frinchaboy, P. M., Kunkel, W. E., Patterson, R. J., & Link, R. 2006, AJ, 131, 375
Whiting, A. B., Hau, G. K. T., Irwin, M., & Verdugo, M. 2007, AJ, 133, 715
Willman, B., Governato, F., Dalcanton, J. J., Reed, D., & Quinn, T. 2004, MNRAS, 353, 639
Willman, B., et al. 2005a, ApJ, 626, L85
———. 2005b, AJ, 129, 2692
———. 2006, AJ, submitted (astro-ph/0603486)
Wu, X. 2007, ApJ, submitted (astro-ph/0702233)
York, D. G., et al. 2000, AJ, 120, 1579
Zentner, A. R., & Bullock, J. S. 2003, ApJ, 598, 49
Zucker, D. B., et al. 2004, ApJ, 612, L121
———. 2006a, ApJ, 643, L103
———. 2006b, ApJ, 650, L41
———. 2007, ApJ, 659, L21